2018

Spatial coherence of light measured by nanoscatt

Saastamoinen, Kimmo

The Optical Society

Tieteelliset aikakauslehtiartikkelit

http://dx.doi.org/10.1364/OPTICA.5.000067

Letter Vol. 5, No. 1 / January 2018 / Optica 67

Spatial coherence of light measured by nanoscattering

Kimmo Saastamoinen,* Lasse-Petteri Leppänen, Ismo Vartiainen, Ari T. Friberg, and Tero Setälä

Institute of Photonics, University of Eastern Finland, P. O. Box 111, FI-80101 Joensuu, Finland
**Corresponding author: kimmo.saastamoinen@uef.fi*

Received 13 September 2017; revised 10 December 2017; accepted 11 December 2017 (Doc. ID 307030); published 18 January 2018

As complex random electromagnetic fields are increasingly exploited in advanced photonics, the measurement of their statistical properties emerges as a crucial technical issue. For spatial coherence, we employ dipole scattering and report on a nano-optics counterpart of Young's interferometer with the openings replaced by metallic dipolar nanoparticles. The results are in agreement with those obtained by other methods. The resolution is comparable to the size of the probes, well beyond that in standard techniques. While we consider here random optical beams, the two-probe method finds particular use in electromagnetic near-field optics where customary polarization elements cannot be employed.

OCIS codes: (030.1640) Coherence; (290.5850) Scattering, particles; (290.5820) Scattering measurements; (120.3180) Interferometry.

https://doi.org/10.1364/OPTICA.5.000067

Spatial coherence is a fundamental property of light traditionally quantified by the visibility of the intensity fringes in Young's double-slit interferometer [1,2]. The experiment has also demonstrated the wave nature of material particles [3,4], and it has played a pivotal role in the research of quantized light [5,6]. Several approaches have been proposed for the determination of spatial coherence of light, including plasmonic devices [7], reversed-wavefront interferometers [8], and digital micromirror devices (DMD) [9].

Quite recently it was predicted that using two nanoparticle probes and observing the visibility of the intensity fringes that their scattered fields produce in the far zone yields the degree of spatial coherence of the light at the particle sites [10]. A single nanoprobe acts as a local scatterer transferring information on the field at the probe, including its statistical characteristics [11], into the far field. In fact, this is the idea of scanning near-field optical microscopy [12], where various probes, such as tapered fiber tips [12] and tips with a nanoparticle at the apex [13,14], have been employed. So far the nanoprobe techniques have only been applied to map the near-field intensity distributions [15,16] and to collect polarimetric information on light beams [17] and three-component optical fields [18–21].

The two-nanoprobe method is analogous to Young's experiment with two diffractive pinholes. While both methods lead to the same physical conclusions, the nanoprobe technique and the double-pinhole interferometer have certain fundamental differences. In the conventional treatment of aperture diffraction, the hole dimensions have to be several wavelengths, whereas the nanoprobes are of subwavelength size. Young's interferometer, therefore, cannot reach the spatial resolution provided by the probe method. In addition, the far fields generated in probe and pinhole techniques are produced by dipole scattering and aperture diffraction, respectively. As shown in [10], the fringe pattern in the former case is equipped with a specific geometric factor. We also note that the use of subwavelength nanoapertures would lead to added complexity, as their far fields depend highly on the material and thickness of the aperture screen as well as on the size of the holes [12].

In this work, we demonstrate the first measurement of the spatial coherence of optical beams with nanoprobes. We consider fully polarized light (allowing scalar treatment), but the technique can be extended to partially polarized beams as well [10]. The probes are gold cube-shaped nanoparticles deposited on a silicon substrate. The results are in excellent agreement with those obtained by traditional methods. This work is a step towards the probing of near-field spatial coherence, and the technique provides a method to acquire the coherence distribution with a subwavelength resolution specified by the probe size.

The setup for measuring the degree of coherence of a light beam with two dipolar nanoprobe particles is depicted in Fig. 1(a). The light sources we consider are a single-mode (spatially coherent, polarized) and a multimode (low spatial coherence, unpolarized) He–Ne laser of wavelength $\lambda = 632.8$ nm. The beams are expanded and collimated in order to obtain tighter focus at the particle site. The light is linearly polarized in the direction of the line passing through both particles, i.e., vertical in our setup. For the latter source, the intensity distribution across the beam is depicted in Fig. 1(b), while Fig. 1(c) shows the intensity profile and the spatial degree of coherence (obtained with a DMD [9]) along the yellow line marked in Fig. 1(b). For the chosen polarization state, the intensity of the dipolar scattering pattern produced by a single nanoparticle is strong at the detector. The beam power after the polarizer was approximately 2.65 mW for both sources. While we consider fully polarized light in this

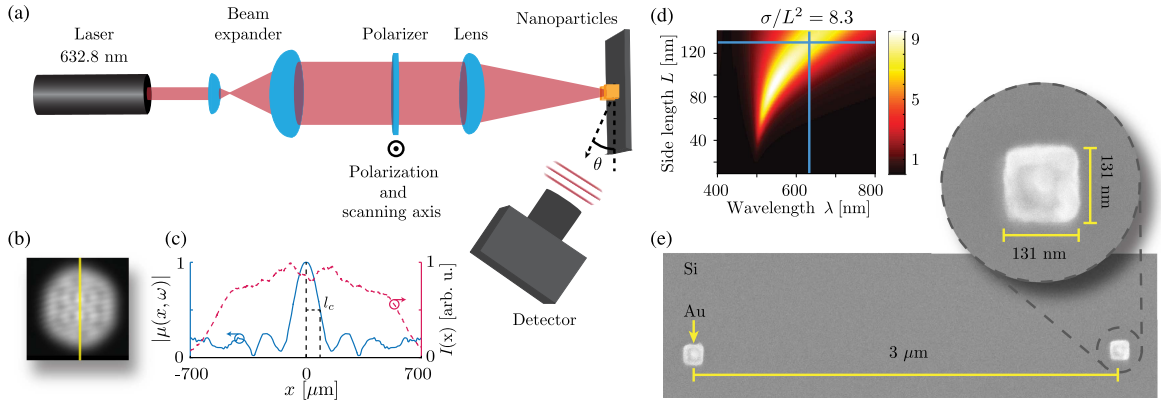

Fig. 1. Two-probe measurement setup. (a) Top view of the geometry. Light from a single-mode or multimode He–Ne laser is expanded, collimated, and polarized vertically. The beam is focused on a pair of gold (Au) nanocubes that act as dipolar scatterers. The far-field interference pattern produced by the particles is recorded at an angle θ to the substrate by moving a photodetector in the vertical direction (parallel to polarization). (b) Intensity distribution across the expanded, unfocused multimode beam. (c) Cross sections of the intensity distribution (red dashed line) and the degree of coherence (blue line) along the yellow line in (b). $l_c = 84$ μm marks the transverse coherence length. (d) Scattering cross section σ of cubic Au particles in terms of the side length L and wavelength λ. The chosen particle size, $L = 130$ nm, and wavelength, $\lambda = 632.8$ nm, are marked with blue lines. (e) SEM image of an actual Au nanocube pair placed on silicon (Si) substrate, with a magnified image of a single cube.

work, the technique can readily be extended to beams of arbitrary states of partial polarization as well [10].

The beams are focused by a lens (30 mm focal length) onto the sample holding the nanoprobes. The resulting intensity spot is approximately 70 μm in diameter (see Beam Focus in Supplement 1), which is still large enough to maintain the beam-like character. The focusing is necessary for two reasons. First, light scattered by the particles is difficult to observe without increasing the incident intensity. Second, the transverse coherence length of the beam should be less than 10 μm at the nanoparticles (since the particle separations are 3–7 μm), which is achieved by scaling (focusing) the coherence width of the multimode laser beam. As Fig. 1(c) indicates, the coherence width of the unfocused beam is approximately 84 μm (degree of coherence is halved from maximum), while focusing scales it by a factor of 20 to approximately 4.2 μm.

The particle pairs are deposited on a silicon substrate (see Particle Fabrication in Supplement 1). We choose cubic gold nanoparticles since their scattering properties (polarizability) are known [22] and they can be accurately fabricated by e-beam lithography. The side length of the nanocubes is chosen as $L \sim 130$ nm in order to get a high scattered power [with the scattering cross section $\sigma/L^2 = 8.3$, as shown in Fig. 1(d)] at the wavelength of 632.8 nm. Moreover, the particles are still small enough to be treated as dipoles [23]. A scanning-electron-microscope (SEM) image of a cube pair and of a single cube are shown in Fig. 1(e). We fabricated sets of nanocube pairs with particle distances of 3, 4, 5, and 7 μm. The small separations guarantee essentially equal intensities at the probe particles. Yet the separations are multiple wavelengths, implying that no considerable propagating or near-field (evanescent) interaction takes place between the probes [12,24].

The scattered far fields generated by the nanoprobes interfere and form an intensity fringe pattern that is observed by moving along the vertical axis a photodetector (Thorlabs PDF10A) located 55 mm from the sample. The intensity fringes and the interaction of the particles with the substrate are carefully analyzed (see Particle–Surface Interaction in Supplement 1). The detector has a square surface area of 1.2 mm^2 (dimensions smaller than the fringe period) and it is capable of measuring signals of femtowatt (fW) power level. We may estimate [11] the scattering power from an individual particle to be about 2.2 pW at the detector. To minimize the stray light caused by backreflections from the focusing lens, the detection angle is set small [$\theta = 20°$, see Fig. 1(a)].

The magnitude of the degree of spatial coherence, $|\mu(\mathbf{r}_1, \mathbf{r}_2, \omega)|$, at the site of the nanoprobes ($\mathbf{r}_1$ and $\mathbf{r}_2$) is obtained from the visibility of the far-field intensity fringes. This is analogous to Young's interferometer, in which the visibility determines the degree of spatial coherence at the two slits [2]. Explicitly the visibility is

$$V = \frac{I_{\max} - I_{\min}}{I_{\max} + I_{\min}} = \frac{2\sqrt{I_1 I_2}}{I_1 + I_2} |\mu(\mathbf{r}_1, \mathbf{r}_2, \omega)|, \tag{1}$$

where $I_{\max}$ and $I_{\min}$ are the neighboring intensity maxima and minima of the fringe pattern, respectively, and I_i, $i \in (1, 2)$, are the field intensities at individual particles. If $I_1 = I_2$, the degree of coherence is simply

$$|\mu(\mathbf{r}_1, \mathbf{r}_2, \omega)| = V, \tag{2}$$

as is the case in our nanoprobe experiments.

We consider first the spatial coherence of the single-mode laser beam by probing the focused field with two nanoprobes separated by $a = 3$ μm. Figure 2(a) shows the measured far-field intensity pattern (black dots), along with a sinusoidal fitting (blue line) as a function of detector position s (a coordinate transverse to the observation direction). The fitting procedure is preceded by background subtraction (see Data Analysis in Supplement 1). The maxima and minima of the fitted intensity curve and Eq. (1) give $V = \mu(\mathbf{r}_1, \mathbf{r}_2, \omega) \approx 0.96$. The degree of spatial coherence is therefore very close to unity, as one would expect for a fully coherent source. Due to the long transverse coherence length, it would not make a noticeable difference if the particle separation were increased (to 4–7 μm), apart from a shorter fringe period. For this reason, we omit the other probe pairs for this source.

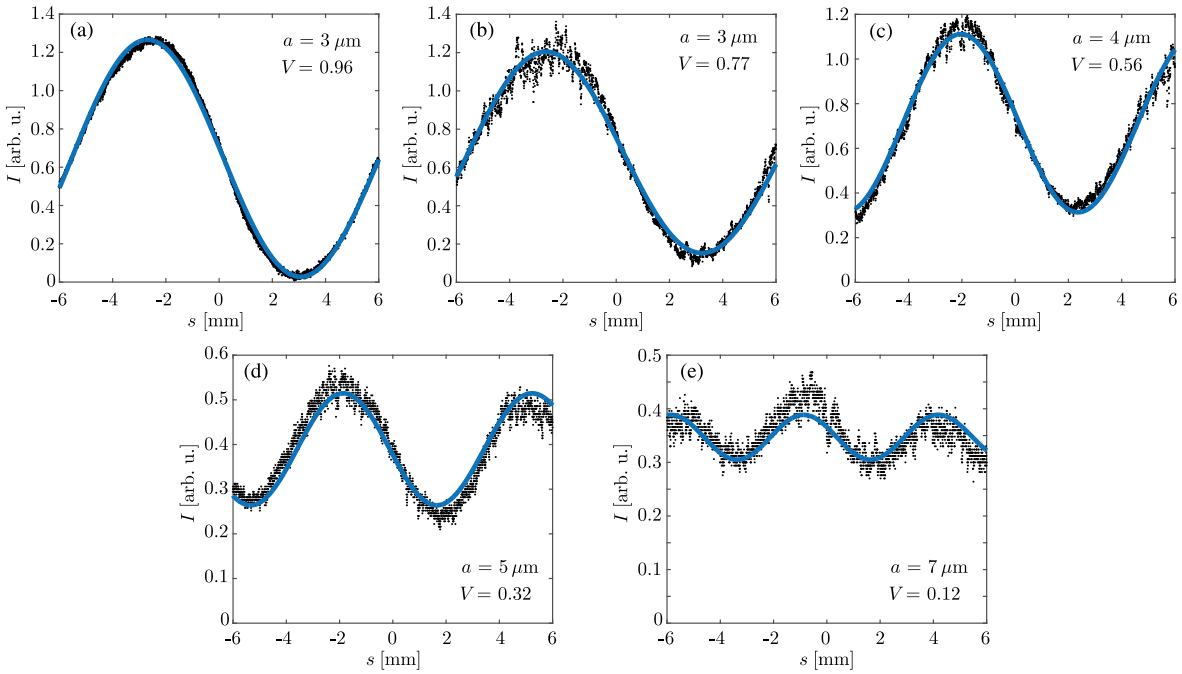

Fig. 2. Illustration of the far-field intensity patterns averaged over several measurements (black dots) and fitted curves (blue solid lines) as a function of the detector position s. (a) Scaled-down (focused) single-mode laser beam when the particles are 3 μm apart. (b)–(e) Scaled multimode laser beam when the particles are separated by a distance of $a = 3$, 4, 5, and 7 μm, respectively.

The situation changes in the case of the multimode laser, since the (scaled down) degree of spatial coherence for that beam is very low. To minimize errors arising from intensity fluctuations at the particle sites, we perform multiple measurements of the same fringe pattern and average the results. The curve fitting is then done for the averaged intensity profile (see Data Analysis in Supplement 1). As a result of this procedure, we present illustrative examples in Figs. 2(b)–2(e) for particle separations $a = 3$, 4, 5, and 7 μm. The corresponding intensity-fringe visibilities are $V = 0.77$, $V = 0.56$, $V = 0.32$, and $V = 0.12$, respectively. We see that for the multimode laser, the visibility of the far-field intensity fringes for the separation of 3 μm, and consequently the degree of coherence at the particle locations, has decreased compared to the single-mode laser. Increasing the particle separation further reduces the visibility and the degree of spatial coherence. Moreover, we observe that the fringe period shortens as the particles are further apart. A similar effect occurs in Young's interferometer when the slit separation is varied.

Through the above procedure, we measured for each particle separation a several intensity-fringe patterns and averaged over them to obtain the degree of coherence. The associated standard deviation provides an error estimate. These are presented in Fig. 3 with colored geometrical objects and bars, respectively. The red cross at $a = 0$ μm corresponds, in fact, to the single-mode laser with $a = 3$ μm, but this coherent case is effectively the same as the multimode laser with a vanishingly small particle separation. To validate our results, the degree of spatial coherence of the multimode laser beam was also obtained with a DMD [9]. However, since it cannot resolve the degree of coherence with a similarly high resolution as the nanoparticle method, we characterize the unfocused beam, and the spatial coherence profile [blue line in Fig. 1(c)] is then scaled down by a factor of 20 to match the focused beam. The ensuing degree of coherence at the particle sites is shown in Fig. 3 by the blue solid curve. The agreement between the two approaches is excellent, demonstrating that the nanoprobe method can provide accurate results.

As the standard deviations suggest, the measurement errors are very small. They arise from various sources, including intensity differences at the probes affecting the visibility, as Eq. (1) shows. However, this effect is minor since the beam is highly uniform on the scale of particle separations. Moreover, any observed random fluctuations in the multimode laser are efficiently averaged out. Other potential error sources are nonuniformities in the particle structures that may occur in the fabrication process. Based on

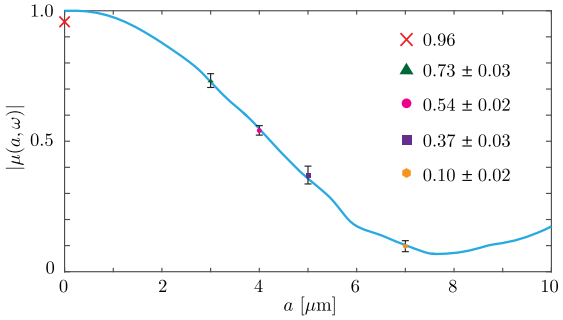

Fig. 3. Measured (average) degrees of spatial coherence for the multimode laser beam. The colored geometrical objects represent the various particle separations a. The solid blue curve shows the degree of coherence of the input beam obtained by a DMD. The resulting degree of coherence profile is scaled down by a factor of 20 to account for the focusing of the beam. The red cross corresponds to the single-mode laser with a 3 μm particle separation, but is here associated with the multimode laser with a vanishingly small particle distance. The errors (black bars) are estimated by computing the standard deviation of multiple measurements.

SEM figures, these effects are small. Measuring the background signal slightly off the particles may also lead to small errors.

We have demonstrated the first-ever probing of the degree of spatial coherence of optical beams in terms of nanoparticle pairs. As probes we have used gold nanocubes with dimensions of 130 nm (strong scattering at HeNe-laser wavelength) and separations of 3–7 μm fabricated on a silicon surface. Similar to the diffractive double pinhole in Young's interferometer, the probes scatter light, the ensuing far-fields interfere, and the visibility of the related intensity-fringe pattern implies the magnitude of the degree of coherence at the particle sites. The results match well to the known spatial coherence profile of the beam.

A drawback of the present method is the low scattering power of the dipole probes, necessitating high beam intensity. This issue is more apparent when the particle separation is increased, since the detection distance has to be longer due to a reduced fringe period. However, the method provides clear advantages. It delivers better spatial resolution (limited by the probe size) and allows access to shorter coherence lengths than the traditional aperture methods. Further, the method can be extended to the near-field domain, where a scanning nanoprobe could reveal the spatial coherence distribution of evanescent waves.

Funding. Magnus Ehrnroothin Säätiö; Itä-Suomen Yliopisto (930350, 931726); Jenny ja Antti Wihurin Rahasto; Academy of Finland (268480, 268705, 308393, 310511).

Acknowledgment. We thank Dr. Henri Partanen for the characterization of the multimode laser with the digital micromirror device. K. S. acknowledges support from the Magnus Ehrnrooth Foundation and L.-P. L. from the Jenny and Antti Wihuri Foundation.

See Supplement 1 for supporting content.

REFERENCES

1. T. Young, Philos. Trans. R. Soc. London **94**, 1 (1804).
2. L. Mandel and E. Wolf, *Optical Coherence and Quantum Optics* (Cambridge University, 1995).
3. C. Jönsson, Z. Phys. **161**, 454 (1961).
4. O. Carnal and J. Mlynek, Phys. Rev. Lett. **66**, 2689 (1991).
5. Y.-H. Kim, R. Yu, S. P. Kulik, Y. Shih, and M. O. Scully, Phys. Rev. Lett. **84**, 1 (2000).
6. S. Kocsis, B. Braverman, S. Ravets, M. J. Stevens, R. P. Mirin, L. K. Shalm, and A. M. Steinberg, Science **332**, 1170 (2011).
7. D. Morrill, D. Li, and D. Pacifici, Nat. Photonics **10**, 681 (2016).
8. M. Santarsiero and R. Borghi, Opt. Lett. **31**, 861 (2006).
9. H. Partanen, J. Turunen, and J. Tervo, Opt. Lett. **39**, 1034 (2014).
10. L.-P. Leppänen, K. Saastamoinen, A. T. Friberg, and T. Setälä, Opt. Lett. **40**, 2898 (2015).
11. L.-P. Leppänen, A. T. Friberg, and T. Setälä, J. Opt. Soc. Am. A **31**, 1627 (2014).
12. L. Novotny and B. Hecht, *Principles of Nano-Optics* (Cambridge University, 2006).
13. O. Sqalli, I. Utke, P. Hoffmann, and F. Marquis-Weible, J. Appl. Phys. **92**, 1078 (2002).
14. I. U. Vakarelski and K. Higashitani, Langmuir **22**, 2931 (2006).
15. T. Kalkbrenner, M. Ramstein, J. Mlynek, and V. Sandoghdar, J. Microsc. **202**, 72 (2001).
16. Y. De Wilde, F. Formanek, R. Carminati, B. Gralak, P.-A. Lemoine, K. Joulain, J.-P. Mulet, Y. Chen, and J.-J. Greffet, Nature **444**, 740 (2006).
17. L.-P. Leppänen, K. Saastamoinen, J. Lehtolahti, A. T. Friberg, and T. Setälä, Opt. Express **24**, 1472 (2016).
18. R. Dändliker, P. Tortora, L. Vaccaro, and A. Nesci, J. Opt. A **6**, S18 (2004).
19. L. Novotny, M. R. Beversluis, K. S. Youngworth, and T. Brown, Phys. Rev. Lett. **86**, 5251 (2001).
20. K. Lindfors, A. Priimagi, T. Setälä, A. Shevchenko, A. T. Friberg, and M. Kaivola, Nat. Photonics **1**, 228 (2007).
21. T. Bauer, P. Banzer, E. Karimi, S. Orlov, A. Rubano, L. Marrucci, E. Santamato, R. W. Boyd, and G. Leuchs, Science **347**, 964 (2015).
22. E. Massa, S. A. Maier, and V. Giannini, New J. Phys. **15**, 063013 (2013).
23. C. F. Bohren and D. R. Huffman, *Absorption and Scattering of Light by Small Particles* (Wiley, 1983).
24. J. Grondalski and D. F. V. James, Opt. Lett. **28**, 1630 (2003).